HemaSphere

EHA EUROPEAN HEMATOLOGY ASSOCIATION

Letter
Open Access

A Decision-tree Approach to Stratify DLBCL Risk Based on Stromal and Immune Microenvironment Determinants

Gian Maria Zaccaria[1,2,*], Maria Carmela Vegliante[1,*], Giuseppe Mezzolla[3], Marianna Stranieri[3], Giacomo Volpe[1], Nicola Altini[3], Grazia Gargano[1,4,5], Susanna Anita Pappagallo[1], Antonella Bucci[1], Flavia Esposito[4,5], Giuseppina Opinto[1], Felice Clemente[1], Antonio Negri[1], Paolo Mondelli[1], Maria Stella De Candia[1], Vitoantonio Bevilacqua[3], Attilio Guarini[1], Sabino Ciavarella[1]

Correspondence: Gian Maria Zaccaria (g.m.zaccaria@oncologico.bari.it).

In diffuse large B-cell lymphoma (DLBCL), the heterogeneity of response to standard first-line therapy[1] largely relies on the tremendous biological complexity of the disease, claiming for an urgent improvement of our capacity to characterize it at diagnosis to guide treatments. Among emerging prognosticators, peculiar cytotypes of tumor microenvironment (TME) and relative gene sets were shown to predict patients' risk.[2–5] We previously recognized prognostic genes reflecting patterns of stromal (myofibroblasts [Myo]) and immune elements (CD4+ T and dendritic cells) intriguingly associated with macrophages (Mo).[6] These latter as well as the choice of reproducible biomarkers to capture their functional heterogeneity remain an object of intense debate.[7] Starting from the notion that Mo polarization and inflammatory response may be influenced by oxysterol levels via nuclear "Liver X receptors" (LXRs),[8,9] we recently recognized the prognostic role of LXRα (*NR1H3*) in DLBCL, prompting future investigation on new LXR agonists for therapeutic purposes.[10]

Here, we sought to corroborate our previous observations using a decision-tree approach on large independent DLBCL cohorts to refine risk stratification integrating TME and clinical features. In doing so, we validated *NR1H3* as an intriguing M1-Mo-related prognosticator, envisioning its potential as a molecular predictor toward future approaches of Mo-targeting drugs.

[1]*Hematology and Cell Therapy Unit, IRCCS Istituto Tumori "Giovanni Paolo II," Bari, Italy*
[2]*Transfer Technology Office, IRCCS Istituto Tumori "Giovanni Paolo II," Bari, Italy*
[3]*Department of Electrical and Information Engineering, Polytechnic University of Bari, Italy*
[4]*INDAM-GNCS Research Group, Rome, Italy*
[5]*Department of Mathematics, University of Bari Aldo Moro, Italy*
**GMZ and MCV equally contributed to this study.*
The authors affiliated to the IRCCS Istituto Tumori "Giovanni Paolo II," Bari, are responsible for the views expressed in this article, which do not necessarily represent the Institute.
Supplemental digital content is available for this article.
Copyright © 2023 the Author(s). Published by Wolters Kluwer Health, Inc. on behalf of the European Hematology Association. This is an open access article distributed under the Creative Commons Attribution NoDerivatives License 4.0, which allows for redistribution, commercial and non commercial, as long as it is passed along unchanged and in whole, with credit to the author.
HemaSphere (2023) 7:4(e862).
http://dx.doi.org/10.1097/HS9.0000000000000862.
Received: September 18, 2022 / Accepted: February 6, 2023

We applied the deconvolution algorithm CIBERSORT[4] in combination with a decision tree–based approach on 2 large independent DLBCL cohorts to recognize the most relevant features among clinical and TME prognosticators. The whole methodological pipeline is detailed in Figure 1A.

Briefly, GEP data from 928 DLBCL cases (training set; GSE117556, Table 1) were deconvoluted to quantify the relative percentages of 24 TME cytotypes (Suppl. Table S1, Figure 1B) and dichotomized according to maximally selected rank statistics (*surv_cutpoint* function implemented in *surminer* R package) based on both progression-free survival (PFS) and overall survival (OS). The resulting variables in keeping with known clinical prognosticators (cell of origin [COO] subtypes and revised International Prognostic Index [Rev-IPI]) and other clinical features (gender, age at diagnosis, lactate dehydrogenase > upper limit of normal, Eastern Cooperative Group performance status, Ann Arbor stage, extranodal involvements, and treatment arm) underwent univariate feature selection by applying log-rank and Cox proportional hazard test on PFS and OS (Suppl. Table S2). Then, the selected significant features were included in a recursive decision-tree model (partykit package implemented in R software).[11] To increase the translational power of the model, it was reapplied by substituting prognostic cell types with consistent molecular surrogates (smooth muscle alpha-2 actin encoded by *ACTA2* gene for Myo and *NR1H3* for M1-Mo). The expression values of these 2 genes were dichotomized according to a cutoff identified by maximally selected rank statistics in 2 groups (high or low) before reapplying the recursive model. Finally, we validated the results on an independent case set of 137 DLBCL (GSE98588)[12] (Suppl. material) using Rev-IPI, *ACTA2*, and *NR1H3* expression value dichotomized according to the cutoff previously identified in the training set. To overcome the batch effect on normalization derived from 2 different array platforms, the expression values were properly scaled. To validate our methods, we used the Transparent Reporting of a Multivariable Prediction Model for Individual Prognosis Or Diagnosis (TRIPOD) criteria (Suppl. TRIPOD).

Among all clinical and TME features undergone univariate analysis, only 12 displayed significant association with both PFS and OS (Suppl. Figures S1–S2). As previously observed,[6,7] those cases with higher predominance of M1-Mo (Suppl. Figure S1A–B) and Myo showed significantly longer OS and PFS (Suppl. Figure S1C–D). Our recursive PFS-based model (Figure 1C) recognized the Rev-IPI as the first feature splitting the entire study

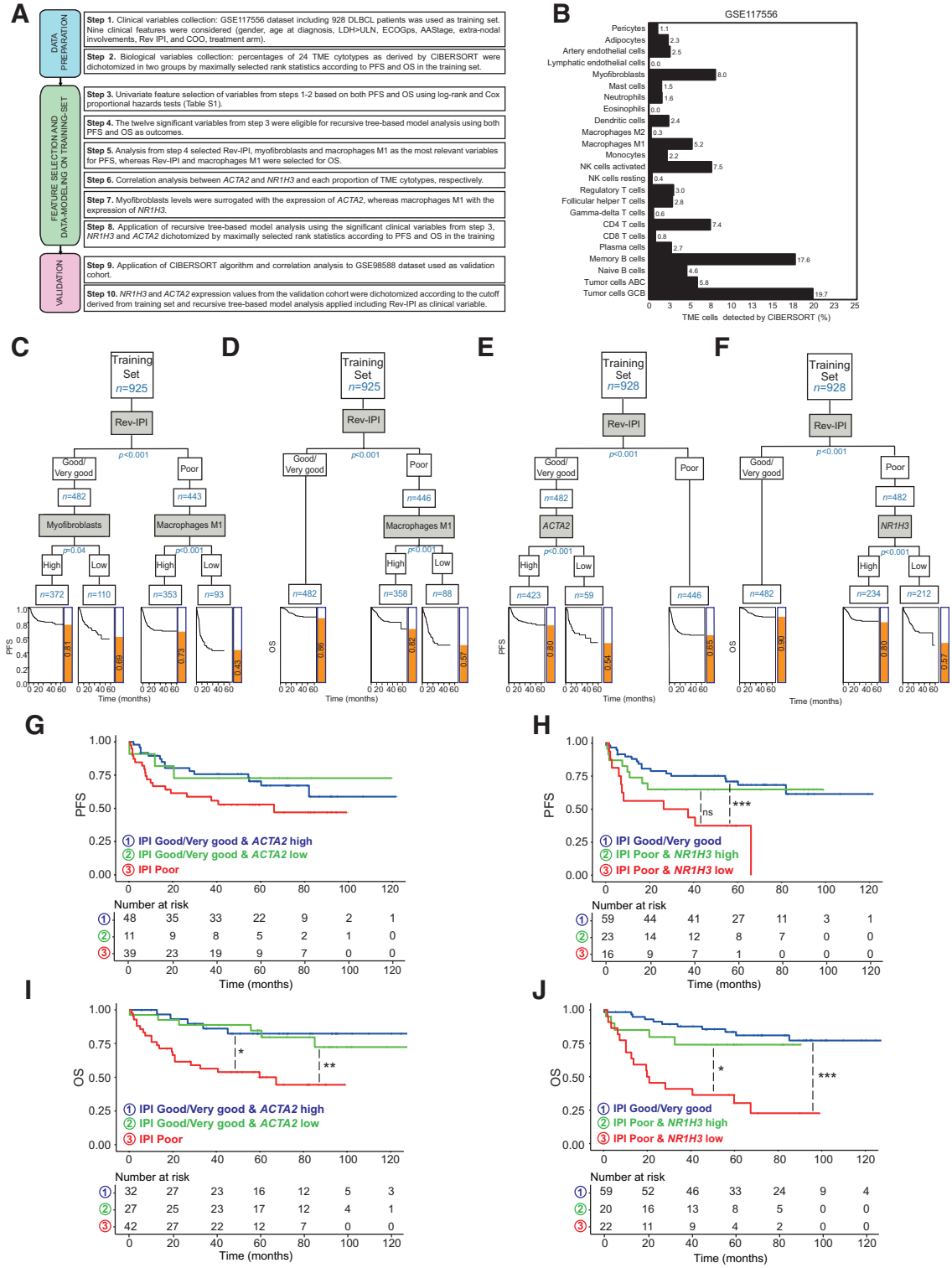

Figure 1. Decision tree–based model combining IPI and TME cells in DLBCL. (A) Schematic description of the pipeline used for data processing. (B) Histograms showing the relative percentages of each cell type in the M24 customized signature as detected by CIBERSORT analysis deconvolution of the GSE117556 dataset (n = 928). Decision-tree depicting results of recursive models applied on clinical and biological features built on PFS (C) and OS (D) in the training set. The most relevant groups are shown along with survival plots (log-rank test, $P < 10^{-3}$). Decision-tree showing results of recursive models applied on clinical features (Rev-IPI variables), *ACTA2 and NR1H3* surrogating Myofibroblasts and M1 macrophages, respectively, built on PFS (E) and OS (F). Most relevant groups are shown along with survival plots (log-rank test, $P < 10^{-3}$). Kaplan-Meier survival plots for PFS (G–H) and OS (I–J) of *ACTA2* and *NR1H3* dichotomized expression combined with Rev-IPI in the validation cohort (GSE98588, n = 98). Adjusted *P* values as derived from pairwise comparisons using log-rank test are shown. ***$P \leq 0.001$; **$P \leq 0.01$; *$P \leq 0.05$; ns (not significant) $P > 0.05$. AAstage = Ann Arbor Stage; ABC = activated B cell; ECOGps = eastern cooperative oncology group performance status; GBC = germinal B center-like; IPI or Rev-IPI = Revised International Prognostic Index; LDH>/≤ULN = lactate dehydrogenase >/≤ upper level of normal; NK = natural killer; OS = overall survival; PFS = progression-free survival; TME = tumor microenvironment.

Table 1

Patients' Characteristics

	Training Set	Validation Set	
No. of patients	**928**	**137**	***P* Value**
Gender, N of males (%)	517 (55.7)	76 (55.5)	1
Age, y: median (IQR)	44.0 (35.0–50.0)	45.5 (36.0–55.0)	*0.018*
LDH > ULN, N (%)	388 (41.8)	52 (50.0)	0.134
ECOGps 3/4, N (%)	105 (11.3)	21 (19.4)	*0.022*
AAStage III/IV, N (%)	638 (68.8)	69 (63.9)	0.35
Extranodal involvement, N (%)	521 (56.1)	28 (25.9)	*<0.001*
Rev IPI (%)			*0.029*
Poor	446 (48.1)	44 (42.3)	
Good	428 (46.1)	47 (45.2)	
Very good	54 (5.8)	13 (12.5)	
NA	0	33	
COO (%)			*<0.001*
ABC	255 (27.5)	63 (46.0)	
GCB	543 (58.5)	54 (39.4)	
UNC	130 (14.0)	20 (14.6)	
Molecular high grade (%)			NA
Double hit/triple hit	35 (9.7)	NA	
MYC-normal	309 (85.8)	NA	
MYC-rearranged	14 (3.9)	NA	
TME cytotypes			
Tumor cells ABC low[a], N (%)	552 (59.5)	109 (79.6)	*<0.001*
Tumor cells ABC low[b], N (%)	552 (59.5)	109 (79.6)	*<0.001*
Tumor cells GCB low[a], N (%)	834 (89.9)	29 (21.2)	*<0.001*
Tumor cells GCB low[b], N (%)	831 (89.5)	29 (21.2)	*<0.001*
Naive B-cells low[a], N (%)	792 (85.3)	87 (63.5)	*<0.001*
Naive B-cells low[b], N (%)	777 (83.7)	106 (77.4)	0.085
Memory B-cells low[a], N (%)	107 (11.5)	94 (68.6)	*<0.001*
Memory B-cells low[b], N (%)	107 (11.5)	19 (13.9)	0.516
Plasma cells low[a], N (%)	237 (25.5)	107 (78.1)	*<0.001*
Plasma cells low[b], N (%)	699 (75.3)	107 (78.1)	0.548
$CD8^+$ cells low[a], N (%)	699 (75.3)	55 (40.1)	*<0.001*
$CD8^+$ cells low[b], N (%)	383 (41.3)	74 (54.0)	*0.007*
$CD4^+$ cells low[a], N (%)	417 (44.9)	77 (56.2)	*0.017*
$CD4^+$ cells low[b], N (%)	680 (73.3)	100 (73.0)	1
Gamma delta TC low[a], N (%)	765 (82.4)	124 (90.5)	*0.024*
Gamma delta TC low[b], N (%)	763 (82.2)	124 (90.5)	*0.021*
Follicular helper TC low[a], N (%)	413 (44.5)	35 (25.5)	*<0.001*
Follicular helper TC low[b], N (%)	504 (54.3)	35 (25.5)	*<0.001*
Regulatory cells low[a], N (%)	518 (55.8)	137 (100.0)	*<0.001*
Regulatory cells low[b], N (%)	808 (87.1)	137 (100.0)	*<0.001*
NK resting low[a], N Low (%)	830 (89.4)	15 (10.9)	*<0.001*
NK resting low[b], N Low (%)	223 (24.0)	28 (20.4)	0.414
NK activated low[a], N (%)	217 (23.4)	0 (0.0)	*<0.001*
NK activated low[b], N (%)	203 (21.9)	40 (29.2)	0.072
Monocytes low[a], N (%)	187 (20.2)	11 (8.0)	*0.001*
Monocytes low[b], N (%)	187 (20.2)	28 (20.4)	1
M1-Mo low[a], N (%)	198 (21.3)	112 (81.8)	<0.001
M1-Mo low[b], N (%)	790 (85.1)	113 (82.5)	0.498
M2-Mo low[a], N (%)	807 (87.0)	56 (40.9)	*<0.001*
M2-Mo low[b], N (%)	0 (0.0)	29 (21.2)	*<0.001*
Dendritic cell low[a], N (%)	0 (0.0)	121 (88.3)	*<0.001*
Dendritic cell low[b], N (%)	0 (0.0)	119 (86.9)	*<0.001*
Eosinophils low[a], N (%)	0 (0)	0 (0)	NA
Eosinophils low[b], N (%)	307 (33.1)	0 (0.0)	*<0.001*
Neutrophils low[a], N (%)	371 (40.0)	0 (0.0)	*<0.001*
Neutrophils low[b], N (%)	824 (88.8)	0 (0.0)	*<0.001*
Myofibroblasts low[a], N (%)	703 (75.8)	113 (82.5)	0.103
Myofibroblasts low[b], N (%)	665 (71.7)	0 (0.0)	*<0.001*
Lymphatic endothelial cells low [a], N (%)	223 (24.0)	0 (0.0)	*<0.001*

(Continued)

Table 1 (Continued)

	Training Set	Validation Set	
No. of patients	**928**	**137**	***P* Value**
Lymphatic endothelial cells low[b], N (%)	0 (0.0)	43 (31.4)	*<0.001*
Artery endothelial cells low[a], N (%)	0 (0.0)	120 (87.6)	*<0.001*
Artery endothelial cells low[b], N (%)	611 (65.8)	110 (80.3)	*0.001*
Adipocytes low[a], N (%)	611 (65.8)	113 (82.5)	*<0.001*
Adipocytes low[b], N (%)	771 (83.1)	113 (82.5)	0.958
Pericytes low[a], N (%)	193 (20.8)	118 (86.1)	*<0.001*
Pericytes low[b], N (%)	813 (87.6)	113 (82.5)	0.127
R-CHOP like chemotherapy, N (%)	113 (12.2)	24 (17.5)	0.108

[a]Cut-off on PFS.

[b]Cut-off on OS.

Italic values represent significant *P* values: $P < 0.05$.

AAStage = Ann Arbor stage; ABC = activated B cell; COO = cell of origin; ECOGps = Eastern Cooperative Group performance status; GCB = germinal center B cell; IPI = international prognostic index; IQR = interquartile range; LDH = lactate dehydrogenase; Mo = macrophages; NA = not available; NK = natural killer; OS = overall survival; PFS = progression-free survival; TME = tumor microenvironment; ULN = upper limit of normal; UNC = unclassified.

cohort into good/very good and poor categories ($P < 0.001$). The more favorable one was further subdivided—according to the level of Myo infiltration—into "high" and "low" subsets differing significantly in terms of PFS ($P = 0.04$). On the other hand, the proportion of intra-tumor M1-Mo (distinct in "high" and "low") was able to separate the poor category into 2 smaller subsets, M1-Mo "high" and "low" ($P < 0.001$), the latter being at worst prognosis, independently of double hit or triple hit (DH/TH) status (Suppl. Figure S3A). Notably, the good/very good and Myo "high" subgroup displayed the best PFS, remarkably longer than cases in the Poor/M1-Mo "low" subgroups. In terms of OS (Figure 1D), our model confirmed the Rev-IPI as main prognosticator ($P < 0.001$) and recognized the extent of M1-Mo infiltration as the only feature identifying—within the poor category—patients at very high risk, independently of DH/TH status (Suppl. Figures S3B). Interestingly, good/very good patients showed OS similar to those that, even belonging to the poor category, have higher M1-Mo infiltration.

Based on our recent finding[6,7] and a new correlation analysis (Suppl. Figure S4A–B), we constructed a decision-tree model using the expression of *ACTA2* and *NR1H3* as molecular surrogates of Myo and M1-Mo, respectively. Again, in the PFS-based model (Figure 1E), the Rev-IPI subdivided patients into good/very good and poor categories ($P < 0.001$). *ACTA2* expression split good/very good patients into 2 additional subgroups with significantly different PFS, while the poor category comprised patients at worse PFS with no further subcategorization. According to OS (Figure 1F), the model confirmed the Rev-IPI as the main risk predictor ($P < 0.001$), showing that the poor category included patients at lower *NR1H3* expression and shortest OS ($P < 0.001$). Notably, despite belonging to the poor category, those expressing higher levels of *NR1H3* displayed similar OS compared with good/very good patients.

We used an independent set[12] of 137 cases to validate these findings. In the univariate and multivariate analysis, *ACTA2* showed no correlation with survival, whereas *NR1H3* displayed a significant prognostic value in terms of both PFS and OS, confirmed also by a multivariate analysis including the Rev-IPI and COO (Suppl. Figure S5). Our PFS-based model categorized patients according to the Rev-IPI and *ACTA2* expression and split only the good/very good cases into 2 additional subclasses with no PFS difference ($P = 0.80$, Figure 1G). Conversely, within the poor category, those at higher *NR1H3* expression showed longer PFS (almost comparable to the good/very good subgroup) (Figure 1H). Consistently, in terms of OS, while *ACTA2* did not show any significant stratification in good/very good cases (Figure 1I), Rev-IPI poor patients with higher expression of *NR1H3* largely overlapped with good/very good patients. On the other hand, the impact of *NR1H3* expression on OS was even more evident for the patients classified as at high risk based on the sole Rev-IPI ($P < 0.001$) (Figure 1J). Moreover, the recursive model including *NR1H3* evaluated on OS (C-index [C] = 0.7, standard error [SE] = 0.04 and Akaike Information Criterion [AIC] = 259.7) outperformed the one on PFS ($C = 0.61$, SE = 0.04, and AIC = 310.9) as well as models including *ACTA2* (PFS, $C = 0.67$, SE = 0.04, and AIC = 267.6 and OS, $C = 0.61$, SE = 0.04, and AIC = 310.9).

Here, we corroborate the prognostic value of peculiar TME components in DLBCL,[6,7] using clinical and transcriptomic data from large patient cohorts to build practical tree-based models of risk stratification. Such an approach may not only enable early prognostication, but also help in enriching a subset of patients who might benefit from new therapeutic opportunities.

Beyond confirming the prognostic value of the Rev-IPI, we pointed out Myo and M1-Mo as key features associated with outcomes, independently of DH/TH status. In particular, we validated (i) a direct correlation between stromal cell infiltration and longer PFS in Rev-IPI favorable patients; and (ii) the capacity of M1-Mo infiltration extent to mitigate (when higher) the outcome of patients at high clinical risk and, conversely, to recognize (when lower) those at very high risk, in terms of both PFS and OS.

Recent deconvolution analyses of TME revealed intriguing association of cellular ecosystems with patients' survival, highlighting on the one hand the prognostic relevance of complex interactions between different immune/stromal elements and, on the other, a recurrent enrichment of fibroblast- and Mo-related signatures in those subsets of DLBCL at relatively favorable prognosis.[13,14] Moreover, these results remain of arguable translational value due to the lack of (i) definite mechanistic relationships between TME cells and outcomes, and (ii) robust functional biomarkers to be incorporated in practical models of risk prediction. Our previous[7] and present results provide novel insights on the latter point, supporting the potential usefulness of *NR1H3* and *ACTA2* as functional prognostic biomarkers related to specific TME components, namely M1-Mo and myofibroblasts, respectively. Our unsupervised model supports the capacity of *NR1H3* to identify more favorable cases at higher expression, while recognizing patients at very high risk and lower expression. We envision a potential relevance of such results in guiding future strategies of Mo-targeted immunomodulation,[10] although they still require a comprehensive mechanistic explanation that takes into account the impact of different immune and/or stromal elements on tumor behavior. Moreover, despite the current lacking of an independent real-world validation, we believe that the broad availability of platforms for the routine measurement of target genes (ie, NanoString Technology) could add translational value to our results in the future, thus prompting the generation of new rationales for TME-oriented therapeutics.

On the other hand, our findings confirm the Rev-IPI as the main prognosticator in DLBCL. However, as compared with previous studies based on canonical regression or machine-learning models,[15] we highlight here the practical advantage of a tree-based approach in improving the accuracy of risk stratification by easily combining well-known and novel prognostic determinants.

In conclusion, we provided evidence that the assessment of stromal and Mo-related features of DLBCL may be of practical help for identifying patients at higher risk, independently of classical prognosticators. Future studies are needed to (i) mechanistically clarify the prognostic significance of TME-related features; (ii) explore their biological meaning, and (iii) integrate them with tumor-related features for a practical improvement of prognostication and, hopefully, therapeutic prediction in DLBCL.

ACKNOWLEDGMENTS

The authors thank the Scientific Director, Prof. Massimo Tommasino, and the clinicians of the Hematology Unit at the IRCCS Istituto Tumori "Giovanni Paolo II." GMZ would thank the colleagues Eng. Giuseppe Carella, Eng. Vito Angiulli, and Eng. G. Salomone from the Technology Transfer Office.

AUTHOR CONTRIBUTIONS

GMZ, MCV, and SC had the idea and designed the manuscript. GMZ, MCV, GM, MS analyzed the data. GMZ, MCV, GV, and SC wrote the manuscript. GV, NA, GG, ASP, AB, FE, GO, FC, AN, PM, MCDC, VAB, and AG reviewed the results, suggested modifications, and approved the final publication.

DATA AVAILABILITY

Data set information can be found in the supplementary digital content.

DISCLOSURES

The authors have no conflicts of interest to disclose.

SOURCES OF FUNDING

Italian Ministry of Health - "Ricerca Corrente 2023."

REFERENCES

1. Coiffier B, Thieblemont C, van den Neste E, et al. Long-term outcome of patients in the LNH-98.5 trial, the first randomized study comparing rituximab-CHOP to standard CHOP chemotherapy in DLBCL patients: a study by the Groupe d'Etudes des Lymphomes de l'Adulte. *Blood*. 2010;116:2040–2045.
2. Lenz G, Wright G, Dave SS, et al. Stromal gene signatures in large-B-cell lymphomas. *N Engl J Med*. 2008;359:2313–2323.
3. Zaitsev A, Chelushkin M, Dyikanov D, et al. Precise reconstruction of the TME using bulk RNA-seq and a machine learning algorithm trained on artificial transcriptomes. *Cancer Cell*. 2022;40:879–894.e16.
4. Newman AM, Liu CL, Green MR, et al. Robust enumeration of cell subsets from tissue expression profiles. *Nat Methods*. 2015;12:453–457.
5. Staiger AM, Altenbuchinger M, Ziepert M, et al. A novel lymphoma-associated macrophage interaction signature (LAMIS) provides robust risk prognostication in diffuse large B-cell lymphoma clinical trial cohorts of the DSHNHL. *Leukemia*. 2020;34:543–552.
6. Ciavarella S, Vegliante MC, Fabbri M, et al. Dissection of DLBCL microenvironment provides a gene expression-based predictor of survival applicable to formalin-fixed paraffin-embedded tissue. *Ann Oncol*. 2018;29:2363–2370.
7. Vegliante MC, Mazzara S, Zaccaria GM, et al. NR1H3 (LXRα) is associated with pro-inflammatory macrophages, predicts survival and suggests potential therapeutic rationales in diffuse large b-cell lymphoma. *Hematol Oncol*. 2022;40:864–875.
8. O'Neill LAJ, Pearce EJ. Immunometabolism governs dendritic cell and macrophage function. *J Exp Med*. 2016;213:15–23.
9. A-González N, Castrillo A. Liver X receptors as regulators of macrophage inflammatory and metabolic pathways. *Biochim Biophys Acta*. 2011;1812:982–994.
10. Mita MM, Mita AC, Chmielowski B, et al. Pharmacodynamic and clinical activity of RGX-104, a first-in-class immunotherapy targeting the liver-X nuclear hormone receptor (LXR), in patients with refractory malignancies. *J Clin Oncol*. 2018;36(15_suppl):3095–3095.
11. Hothorn T, Zeileis A, Cheng E, et al. partykit: a modular toolkit for recursive partytioning in R. *J Mach Learn Res*. 2015;16:3905–3909. Available at: http://CRAN.R-project.org/package=. Accessed September 16, 2022.
12. Chapuy B, Stewart C, Dunford AJ, et al. Molecular subtypes of diffuse large B cell lymphoma are associated with distinct pathogenic mechanisms and outcomes. *Nat Med*. 2018;24:679–690.
13. Kotlov N, Bagaev A, Revuelta MV, et al. Clinical and biological subtypes of b-cell lymphoma revealed by microenvironmental signatures. *Cancer Discov*. 2021;11:1468–1489.
14. Steen C. An atlas of clinically-distinct tumor cellular ecosystems in diffuse large B cell lymphoma. December 2019. Available at: https://ash.confex.com/ash/2019/webprogram/Paper129461.html. Accessed December 19, 2019.
15. Biccler JL, Eloranta S, de Nully Brown P, et al. Optimizing outcome prediction in diffuse large B-cell lymphoma by use of machine learning and nationwide lymphoma registries: a Nordic Lymphoma Group Study. *JCO Clin Cancer Inform*. 2018;2:1–13.